A Three-Mass Tethered System for Micro-g/Variable-g Applications

Enrico C. Lorenzini*
Harvard-Smithsonian Center for Astrophysics, Cambridge, Massachusetts

This paper describes a Space-Station-attached tethered system for micro-g/variable-g applications. The system consists of three platforms: the Space Station, an end mass anchored at the end of a 10-km-long kevlar tether, and a micro-g/variable-g laboratory with the capability of crawling along the tether. Control strategies are devised for performing both the deployment and the stationkeeping maneuvers of the system. Effective algorithms are identified for damping out the major oscillations of the system.

Nomenclature

a	= semimajor axis
A_i	= ith tether cross section
E_i	= ith tether Young's modulus
F_i	= force acting upon the ith mass
g	= gravity acceleration at the Earth's surface
k_{ti}	= ith-tether stiffness
l_i	= distance between mass m_i and mass m_{i+1}
m_i	= ith mass
r_i	= radius vector from the Earth's center to the ith mass
T_i	= tension in the ith tether
x,z	= orbiting axes
x_B,z_B	= body axes
x_I,z_I	= inertial axes
Ω	= orbital rate
ρ_i	= radius vector from the system center of mass to the ith mass

Introduction

THE ongoing development of the Space Station program has vitalized research in microgravity related experiments. Material processing, pharmaceutical production, and life sciences are the disciplines that will benefit the most from an orbiting laboratory capable of providing a microgravity acceleration level (or better) at frequency <0.1 Hz for 1 day to 1 month duration.[1,2] The current requirements for the microgravity laboratory on board the Space Station specify a 10^{-5} g acceleration level at all frequencies.[3] This acceleration level is marginally satisfactory for most of the envisioned microgravity experiments. Furthermore, the microgravity experiments severely restrict the scheduling of other "noisy" activities onboard the Space Station. The reasons above prompted us to conceive an alternative configuration for the microgravity laboratory that makes use of a tethered system attached to the Space Station.[4,5] As shown in Fig. 1 the system consists of a 10-km-long, 2-mm-diameter kevlar tether attached to the Station at one end. Another platform (e.g., a scientific platform) with a presently estimated mass of 9.06 metric tons is attached to the other end of the tether. The micro-g/variable-g laboratory (in short, "g-laboratory" or "g-platform") with an estimated mass of 5 metric tons is also attached to the tether in between the two end platforms. The g-laboratory is equipped with a mechanism for "crawling" along the tether from one end to the other. The stable configuration of the system, as thoroughly dealt with in other papers,[6,7] is along the local vertical while the tether is stretched by opposite forces resulting from the balance of gravitational and centrifugal forces acting upon the system. The point where the above-mentioned forces balance out is often called "orbit center" and its distance from the Earth's center, when the tether mass is neglected, is given by

$$r_0 = \left(\sum_{i=1}^{3} m_i r_i \Big/ \sum_{i=1}^{3} m_i / r_i^2 \right)^{1/3} \tag{1}$$

where r_i is the length of the radius vector from the ith mass to the Earth's center and the summation is extended to the three masses which constitute the system. For moderately long systems the orbit center coincides with the center of gravity and with the center of mass (C.M.). In our case, assuming a Space Station mass of 90.6 metric tons (as foreseen for the initial phase of the Space Station program), the offset between the center of mass and the orbit center is 1.2 m when the g-laboratory is located at the orbit center and the Space Station is flying at 500 km altitude. If the laboratory is displaced from the orbit center it will experience a steady-state acceleration, linearly dependent upon the distance from the orbit center ℓ_{oc}, the modulus of which is given by

$$A_g = 3\Omega^2 l_{oc} \tag{2}$$

This acceleration is usually called gravity gradient acceleration but actually two thirds of it originates from gravitational forces and one third from centrifugal forces.

It follows from the description above that by placing the g-platform at various distances from the orbit center, the g-laboratory will experience correspondingly different accelerations ranging from zero-g at the orbit center to approximately $10^{-2}g$ at the tether end opposite the Station.

Once the system is deployed from the Space Station the residual oscillations (e.g., vibrations excited during the deployment phase) must be damped out by active and/or passive dampers. Both the deployment maneuver and the damping algorithms activated during the stationkeeping phase are described in the next sections.

Mathematical Models

Two reference frames are erected (see Fig. 1). The orbiting reference frame $[x,z]$ rotates at constant orbital rate Ω. Its origin coincides with the system (C.M.) at time $t=0$ with the z axis along the local vertical toward the Earth's center, and the

Received June 11, 1986; presented as Paper 86-1990 at the AIAA/AAS Guidance, Navigation and Control Conference, Williamsburg, VA, Aug. 18-20, 1986; revision received Dec. 16, 1986.

*Scientist, Radio and Geoastronomy Division.

x axis along the local horizon on the orbital plane toward the direction of flight.

The body reference frame $[x_B, z_B]$ has its origin at the system C.M., with the z_B axis parallel to the line through the end masses (m_1 and m_3) of the system and pointing toward m_1, and the x_B axis on the orbital plane toward the direction of flight.

Two different mathematical models have been derived for the dynamics of the system based on different choices for the integration variables. Both models describe the two-dimensional dynamics (in the orbital plane) with respect to the orbiting reference frame. The assumptions are the same for the two models: point masses, spherical Earth, second-order expansion of the gravity potential, elastic but massless tethers. In the first model, moreover, the orbit of the system C.M. is assumed to be circular.

Mathematical model 1 makes use of the Lagrangian coordinates θ, l_1, l_2, ϵ (see Fig. 1). The kinetic energy of the system is given by

$$T=\frac{1}{2}\sum_{i=1}^{3} m_i |v_{Ii}|^2 \tag{3}$$

where the inertial velocity v_n can be expressed in the orbiting reference frame as follows:

$$v_{Ii}=v_{Bi}+\Omega\times a+(\dot{\theta}+\Omega)\times\rho_{Bi} \tag{4}$$

In Eq. (4) the subscript B identifies the body reference frame. By developing Eq. (4) and by substituting in Eq. (3) we get:

$$T=\frac{1}{2}\sum_{i=1}^{3} m_i\Big\{\dot{x}_{Bi}^2+\dot{z}_{Bi}^2+(\dot{\theta}-\Omega)^2(x_{Bi}^2+z_{Bi}^2) +2(\dot{\theta}-\Omega)(\dot{x}_{Bi}z_{Bi}-x_{Bi}\dot{z}_{Bi})\Big\}+\frac{1}{2}m_{tot}\Omega^2a^2 \tag{5}$$

where $m_{tot}=m_1+m_2+m_3$ expresses the total mass of the system.

$$V=-\mu\sum_{i=1}^{3}\frac{m_i}{|r_i|} \tag{6}$$

The potential energy expansion, with respect to the body axes, truncated to the second order gives

$$V=-\frac{1}{2}\sum_{i=1}^{3} m_i\Omega^2\Big\{(3\cos^2\theta-1)z_{Bi}^2+(3\sin^2\theta-1)x_{Bi}^2 -6\sin\theta\cos\theta x_{Bi}z_{Bi}\Big\}-m_{tot}\Omega^2a^2 \tag{7}$$

Since $\epsilon \ll l_i$ we can express x_{Bi}, z_{Bi} in terms of l_i and ϵ as follows:

$$\begin{aligned} z_{B1}&=R_3l_2+(1-R_1)l_1\\ z_{B2}&=R_3l_2-R_1l_1\\ z_{B3}&=(R_3-1)l_2-R_1l_1\\ x_{B1}&=-R_2\epsilon\\ x_{B2}&=(1-R_2)\epsilon\\ x_{B3}&=-R_2\epsilon \end{aligned} \tag{8}$$

where $R_i=m_i/m_{tot}$.

The Lagrangian function L is readily obtained by subtracting the potential energy from the kinetic energy, while the equations of motion are given by

$$\frac{d}{dt}\left(\frac{\partial L}{\partial\dot{q}_i}\right)-\frac{\partial L}{\partial q_i}=Q_{qi}, \qquad i=1,\ldots,4 \tag{9}$$

where the Lagrangian coordinates are

$$q_1=\theta;\ q_2=\epsilon;\ q_3=l_1;\ q_4=l_2 \tag{10}$$

Substitution of Eqs. (8) into Eqs. (5) and (7) gives the Lagrangian as a function of the variables l_1, l_2, ϵ, θ. After lengthy derivatives we get the following equations of motion:

$$\begin{aligned} &\ddot{\theta}\{R_1l_1[l_1+u]+R_3l_2[l_2-u]+R_2(1-R_2)\epsilon^2\}\\ &\quad+2(\dot{\theta}-\Omega)\{R_1l_1[\dot{l}_1+\dot{u}]+R_3l_2[\dot{l}_2-\dot{u}]\\ &\quad+R_2(1-R_2)\epsilon\dot{\epsilon}\}+3\Omega^2\sin\theta\cos\theta\{R_1l_1[l_1+u]\\ &\quad+R_3l_2[l_2-u]-R_2(1-R_2)\epsilon^2\}+3\Omega^2(\sin^2\theta\\ &\quad-\cos^2\theta)R_2u\epsilon-R_2\epsilon\{R_1\ddot{l}_1-R_3\ddot{l}_2\}-R_2\ddot{\epsilon}u=Q_\theta/m_{tot}\\ &R_2(1-R_2)[\ddot{\epsilon}+g\epsilon]-2(\dot{\theta}-\Omega)R_2\dot{u}\\ &\quad-(\ddot{\theta}+d)R_2u=Q_\epsilon/m_{tot}\\ &R_1(1-R_1)[\ddot{l}_1+bl_1]+R_1R_3[\ddot{l}_2+bl_2]\\ &\quad-2(\dot{\theta}-\Omega)R_1R_2\dot{\epsilon}-(\ddot{\theta}-d)R_1R_2\epsilon=Q_{l_1}/m_{tot}\\ &R_3(1-R_3)[\ddot{l}_2+bl_2]+R_1R_3[\ddot{l}_1+bl_1]\\ &\quad+2(\dot{\theta}-\Omega)R_2R_3\dot{\epsilon}+(\ddot{\theta}-d)R_2R_3\epsilon=Q_{l_2}/m_{tot} \end{aligned} \tag{11}$$

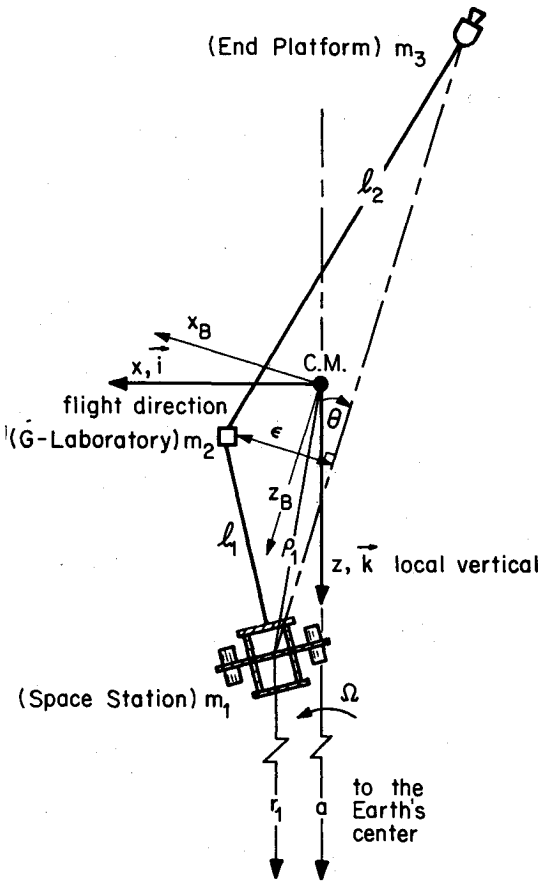

Fig. 1 Schematic of three-mass tethered system.

where

$$b=\Omega^2(1-3\cos^2\theta)-(\dot\theta-\Omega)^2$$

$$d=3\Omega^2\sin\theta\cos\theta$$

$$g=\Omega^2(1-3\sin^2\theta)-(\dot\theta-\Omega)^2 \tag{12}$$

while u is the distance of m_2 from the system C.M. and $\dot u$ is the associated rate of change given respectively by

$$u=R_3l_2-R_1l_1$$

$$\dot u=R_3\dot l_2-R_1\dot l_1 \tag{13}$$

The generalized forces in Eqs. (11) are given by

$$Q_j=\sum_{i=1}^{3}F_i\frac{\partial r_i}{\partial q_j},\qquad j=1,\ldots,4 \tag{14}$$

where F_i are the forces acting upon the three masses. Since $\epsilon_i\ll l_i$, we have that $\sin(\epsilon_i/l_i)\simeq\epsilon_i/l_i$ and $\cos(\epsilon_i/l_i)\simeq 1$. The forces F_i are therefore given by:

$$F_1=-T_1(\cos\theta+\epsilon/l_1\sin\theta)k$$

$$-T_1(\sin\theta-\epsilon/l_1\cos\theta)i$$

$$F_2=[(T_1-T_2)\cos\theta+(T_1/l_1+T_2/l_2)\epsilon\sin\theta]k$$

$$+[(T_1-T_2)\sin\theta-(T_1/l_1+T_2/l_2)\epsilon\cos\theta]i$$

$$F_3=T_2(\cos\theta-\epsilon/l_2\sin\theta)k$$

$$+T_2(\sin\theta+\epsilon/l_2\cos\theta)i \tag{15}$$

where T_1 and T_2 are the tensions in tethers 1 and 2, respectively. The radius vectors r_i are given by

$$r_i=x_ii+z_ik$$

$$=(z_{Bi}\sin\theta+x_{Bi}\cos\theta)i$$

$$+(z_{Bi}\cos\theta-x_{Bi}\sin\theta)k,\qquad 1=1,2,3 \tag{16}$$

By using Eqs. (8) and by substituting Eqs. (15) and (16) into Eq. (14) we finally get

$$Q_\theta=0$$

$$Q_\epsilon=-\epsilon(T_1/l_1+T_2/l_2)$$

$$Q_{l1}=-T_1$$

$$Q_{l2}=-T_2 \tag{17}$$

Since Eqs. (11) are of the form $A\ddot x=b(x,\dot x)$ the coefficient matrix A must be inverted in order to integrate numerically the equations of motion.

In mathematical model 2 the integration variables are the Cartesian coordinates of the masses with respect to the above-mentioned orbiting reference frame. The variables l_1, l_2, ϵ, θ are then obtained from the Cartesian coordinates. The assumptions for model 2 are the same as those of model 1 except for the circularity of the orbit. With reference to Fig. 1, the inertial acceleration of the ith *mass* with respect to the rotating orbiting frame is given by

$$\ddot r_{Ii}=\ddot\rho_i+2\Omega\times\dot\rho_i+\Omega\times(\Omega+r_i),\qquad i=1,2,3 \tag{18}$$

The equations of motion in functional form are given by

$$m_i\ddot r_{Ii}=F_{gi}+F_{Ti},\qquad i=1,2,3 \tag{19}$$

where F_{gi} is the gravity force acting upon the ith *mass* given by

$$F_{gi}=-\nabla V_i=-\nabla\left\{\tfrac{1}{2}m_i[2\Omega^2a^2+2\Omega^2az_i-\Omega^2(x_i^2+z_i^2)+3\Omega^2z_i^2]\right\} \tag{20}$$

while F_{Ti} is the total tension acting upon the ith *mass*. By developing Eqs. (18–20) we obtain the well-known Hill's equations as follows:

$$\ddot x_i-2\Omega\dot z_i=F_{Txi}/m_i,\qquad i=1,2,3$$

$$\ddot z_i-3\Omega^2z_i+2\Omega\dot x_i=F_{Tzi}/m_i,\qquad i=1,2,3 \tag{21}$$

With reference to Fig. 2 we derive the force F_{Ti} as follows:

$$F_{Ti}=[T_{xi}+T_{x,i-1}]i+[T_{zi}-T_{z,i-1}]k,\qquad i=1,2,3 \tag{22}$$

where T_{xi}, T_{zi} are the components of the tension T_i in the tether connecting the ith *mass* to the $i+1$th *mass*, given by

$$T_{xi}=T_i\cos\beta_i=T_i(x_{i+1}-x_i)/l_i,\qquad i=1,2$$

$$T_{zi}=T_i\sin\beta_i=T_i(z_{i+1}-z_i)/l_i,\qquad i=1,2 \tag{23}$$

while $T_{x3}=T_{z3}=0$. The relations between l_1, l_2, θ, ϵ and the integration variables can be easily computed as follows:

$$\theta=\tan^{-1}\left\{\frac{x_1-x_3}{z_1-z_3}\right\}$$

$$l_i=[(x_{i+1}-x_i)^2+(z_{i+1}-z_i)^2]^{1/2},\qquad i=1,2 \tag{24}$$

The lateral displacement ϵ is derived by computing the coordinates of the point of intersection (x_c, z_c) between the straight line through m_1 and m_3 and its perpendicular through m_2. The result is as follows:

$$\epsilon=[(x_2-x_c)^2+(z_2-z_c)^2]^{1/2}\,\mathrm{sign}(x_2-x_c) \tag{25}$$

where

$$x_c=[x_1-x_2\tan^2\theta+(z_2-z_1)\tan\theta]/(1-\tan^2\theta)$$

$$z_c=[x_c-x_2]\tan\theta-z_2 \tag{26}$$

In both models 1 and 2 the tension in each tether is computed from the tether stretch. A longitudinal oscillation damper (along the tether) with stiffness k_i and damping b_i has been added to each tether segment. In Fig. 2, l_{ci} is the commanded length of the ith tether that can follow a prescribed control law if the associated tether is actually controlled by a reel system or if not, it is the natural tether length, l_{di} is the length of the associated longitudinal damper and l_{ti} the ith *tether* stretch. Tether tensions and stretches of the longitudinal dampers for the three-mass system are therefore as follows:

$$T_i=k_{ti}l_{ti}=\frac{E_iA_i}{l_{ci}}(l_i-l_{di}-l_{ci}),\qquad i=1,2$$

$$\dot l_{di}=\frac{k_{ti}}{b_i}l_{ti}-\frac{k_i}{b_i}l_{di},\qquad i=1,2 \tag{27}$$

Both models 1 and 2 have been numerically integrated by using a fourth-order Runge-Kutta integrator with variable step

size. Results for test cases with circular orbit of the system C.M. have been identical, demonstrating the reliability of the models.

Model 1 is suitable for analytical simplifications which provide direct insights into the dynamics of the system. Model 2 does not have this feature but can be more efficiently integrated than model 1 (especially with more than three masses) because it does not require any matrix inversion. The equations of motion of model 2 are summarized below:

$$\ddot{x}_1 = 2\Omega\dot{z}_1 + T_1(x_2 - x_1)/(m_1 l_1)$$

$$\ddot{x}_2 = 2\Omega\dot{z}_2 + T_2(x_3 - x_2)/(m_2 l_2) + T_1(x_1 - x_2)/(m_2 l_1)$$

$$\ddot{x}_3 = 2\Omega\dot{z}_3 + T_2(x_2 - x_3)/(m_3 l_2)$$

$$\ddot{z}_1 = 3\Omega^2 z_1 - 2\Omega\dot{x}_1 + T_1(z_2 - z_1)/(m_1 l_1)$$

$$\ddot{z}_2 = 3\Omega^2 z_2 - 2\Omega\dot{x}_2 + T_2(z_3 - z_2)/(m_2 l_2) + T_1(z_1 - z_2)/(m_2 l_1)$$

$$\ddot{z}_3 = 3\Omega^2 z_3 - 2\Omega\dot{x}_3 + T_2(z_2 - z_3)/(m_3 l_2) \qquad (28)$$

where, for equal cross sections and Young's moduli of the two tethers, we have

$$T_1 = EAl_{t1}/l_{c1}$$

$$T_2 = EAl_{t2}/l_{c2}$$

$$l_{t1} = l_1 - l_{d1} - l_{c1}$$

$$l_{t2} = l_2 - l_{d2} - l_{c2}$$

$$\dot{l}_{d1} = k_{t1}l_{t1}/b_1 - k_1 l_{d1}/b_1$$

$$\dot{l}_{d2} = k_{t2}l_{t2}/b_2 - k_2 l_{d2}/b_2 \qquad (29)$$

Equations (28) and (29) together with Eqs. (24-26) describe the two-dimensional dynamics of the three-mass tethered system.

Damping Algorithms

Before dealing with the deployment maneuvers of the three-mass system we must conceive effective algorithms for damping out the oscillations associated with the various degrees of freedom of the system; namely, the libration θ, the lateral oscillation ϵ, and the longitudinal oscillations l_1, l_2.

Libration/Lateral Dampers

From Eq. (11) we can infer that the libration of the system, when the g-laboratory m_2 is placed at the system C.M. ($m_1 l_1 = m_3 l_2$), is described in first approximation, for small oscillations, by the following simplified equation

$$\ddot{\theta} l^2 - 2(\dot{\theta} - \Omega)l\dot{l} + 3\Omega^2 l^2\theta = 0 \qquad (30)$$

where $l = l_1 + l_2$. We assume, moreover, that the tether is unstretchable; hence $l = l_c$.

In Eq. (30) the second is the dissipative term. The energy dissipated for each libration cycle is therefore given by

$$E_d = 2\int_0^\tau l\dot{l}(\dot{\theta} - \Omega)\dot{\theta}\,dt$$

$$\simeq 2l_0\int_0^\tau \dot{l}(\dot{\theta} - \Omega)\dot{\theta}\,dt \qquad (31)$$

where $\tau = 2\pi/(\sqrt{3}\Omega)$ is the period of the libration and l_0 is the tether length for $\theta = 0$. Our goal is to implement a tether control law (for the two tethers) that maximizes E_d. Let us adopt the following control law:

$$l_c = l_0(1 - K_\theta\theta) \qquad (32)$$

with the gain K_θ greater than zero. The length control law expressed by Eq. (32) can be readily transformed into a rate control law. Here we adopt the length control formulation because it gives a more immediate insight into the dynamics of the system, as explained later.

Since $d\dot{\theta}^2/dt = 2\dot{\theta}\ddot{\theta}$ and, for small values of θ, $l \simeq l_0$, by multiplying Eq. (30) by $\dot{\theta}$ and integrating from 0 to τ we obtain

$$l_0^2\int_0^\tau d\dot{\theta}^2 + 2l_0\int_0^\tau \dot{l}(\dot{\theta} - \Omega)\dot{\theta}\,dt + 3\Omega^2 l_0^2\int_0^\tau \theta\,d\theta = 0 \qquad (33)$$

For light damping the approximate solution of Eq. (30), over one cycle, is as follows:

$$\theta = \bar{\theta}\sin(\sqrt{3}\Omega t) \qquad (34)$$

where $\bar{\theta}$ is the libration amplitude and $\sqrt{3}\Omega$ the frequency. By substituting Eq. (34), its derivative, and Eq. (32) into equation (33), and after computing the integrals [the third integral in Eq. (33) is equal zero] we finally get

$$\frac{\Delta\bar{\theta}}{\bar{\theta}} \simeq \frac{\pi}{\sqrt{3}\bar{\theta}}\frac{\delta l}{l_0} \qquad (35)$$

where $\delta l = 2l_0 k_\theta\bar{\theta}$ is the peak-to-peak tether length variation as derived from Eq. (32), while $\Delta\bar{\theta}$ is the decrease of libration amplitude per libration cycle. In the case of light damping Eq. (35) expresses the logarithmic decrement of the libration angle. The most important and unique feature of the control law (S-type) expressed in Eq. (35) is that the logarithmic decrement increases inversely with the libration amplitude $\bar{\theta}$. The trajectory followed by the end masses is readily obtained by substituting Eq. (34) into Eq. (32) and solving for the x and z components. It is interesting to note that the trajectory fol-

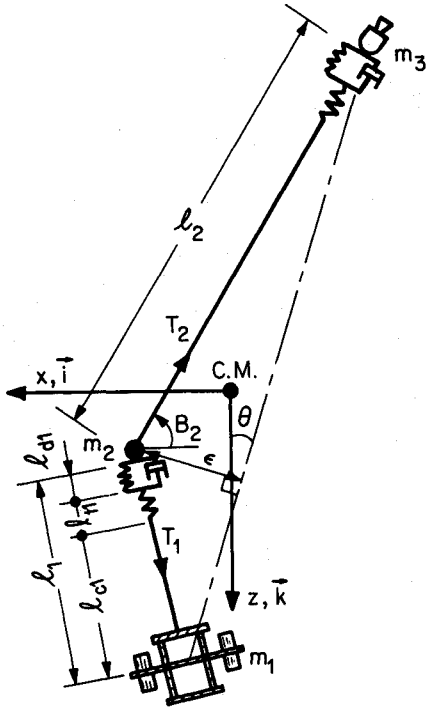

Fig. 2 Schematic of longitudinal dampers.

lowed by the end masses in a damping cycle is not an eight-shaped yo-yo cycle[6,7] but an S-shaped cycle. In other words, the tether is shortened during the retrograde part of the libration and is lengthened during the prograde part as shown in Fig. 3. The control law expressed by Eq. (32) can be adapted to a three-mass system by modifying and generalizing Eq. (32) as follows:

$$l_{c1} = l_{01}[1 - (K_\theta\theta - K_\epsilon\epsilon/l_1)]$$

$$l_{c2} = l_{02}[1 - (K_\theta\theta + K_\epsilon\epsilon/l_2)] \qquad (36)$$

Both θ and ϵ are fed back into the tether reel control. Because of the last terms in Eq. (36) the mass m_2 is moved along the wire in such a way as to produce Coriolis forces which are opposed to the lateral displacement ϵ in order to detract energy from the oscillation associated to that degree of freedom. A simplified version of Eq. (36) can be obtained by assuming $K_\epsilon = K_\theta$, consequently we obtain (see Fig. 3)

$$l_{c1} = l_{01}[1 - K_\theta(\theta - \epsilon/l_1)] = l_{01}(1 - K_\theta\theta_1)$$

$$l_{c2} = l_{02}[1 - K_\theta(\theta + \epsilon/l_2)] = l_{02}(1 - K_\theta\theta_2) \qquad (37)$$

This simplified version, where θ_1 and θ_2 are fed back into the reel control system, is the one adopted in the following simulations. The value of the gain K_θ has been determined by imposing a maximum tether length variation, during a libration damping cycle, of 1% of the fully deployed tether length per degree of libration θ. The lateral oscillation ϵ actually gives a smaller contribution than the libration θ. The resulting value for the gain is $K_\theta = 0.55$.

Longitudinal Dampers

Two passive dampers (spring-dashpot), mounted in series to their respective tethers, have been added to the system for damping the longitudinal tether oscillations. The passive solution has been chosen in order to simplify the design of the three-mass system. According to our design philosophy the reel system (unavoidably massive) controls the low frequency oscillations (librational and lateral) of the system while the passive dampers damp the higher frequency, longitudinal oscillations.

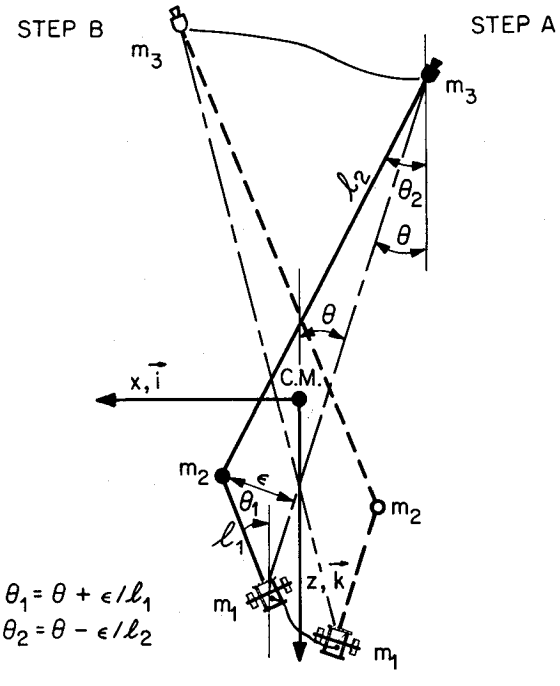

Fig. 3 Pictorial representation of system's dynamics during a libration cycle with librational/lateral dampers switched on.

In order to maximize the energy transfer between the longitudinal vibrations of the tethers and of the respective longitudinal dampers, the natural frequency of each damper must be equal to the natural frequency of the associated tether. Since the longitudinal oscillation frequency changes with tether length the passive dampers perform best for a specific tether length only. An adaptive system could be implemented instead but it has not been included in the present analysis. In the present design each passive damper is tuned to the frequency of the associated 2-mm-diam kevlar tether at the natural tether length during stationkeeping: l_{sk1} and l_{sk2}, respectively. The damping coefficient ξ has been set at 0.9 for both dampers. From numerical simulations $\xi = 0.9$ has proved to maximize the damping of the longitudinal vibrations in the two tether segments. Since mass m_2 is placed at the system C.M., $l_{sk1}m_1 = l_{sk2}m_3$ and the angular frequency of tether 1 is equal to the angular frequency of tether 2, as indicated by

$$\omega_{l1} = \omega_{l2} = [EA/(l_{sk1}m_1)]^{1/2} = 2.74\times10^{-2}\text{rad/s}$$

$$= 4.4\times10^{-3}\text{ Hz} \qquad (38)$$

where $EA = 61645$ N for a 2-mm-diam kevlar tether, $l_{sk1} \simeq 909$ m, and $m_1 = 90.6$ metric tons. Consequently the gains of the longitudinal dampers in Eq. (29) are as follows:

$$k_1 = EA/l_{sk1} = 67.81\text{ N/m}$$

$$k_2 = EA/l_{sk2} = 6.781\text{ N/m}$$

$$b_1 = 2\xi\omega_{l1}m_1 = 4460.24\text{ N/(m/s)}$$

$$b_2 = 2\xi\omega_{l2}m_2 = 446.024\text{ N/(m/s)} \qquad (39)$$

where $l_{sk1}/l_{sk2} = m_3/m_1 = 1/10$. Equation (38) also indicates that the tethers provide a very effective isolation of the g-laboratory from any oscillation of the Space Station or the end platform with a frequency greater than 0.1 Hz.

Deployment Strategy

Deployment of the system is obtained by unwinding the two tethers from two reel systems that control independently tether 1 and tether 2. Equation (30) referes to a two-mass system but it also describes approximately the dynamic of a three-mass system as long as mass m_2 is located at the system C.M. From Eq. (30) we infer that in order to have a deployment with constant θ (deployment along a straight line) the reeled out tether length must be an exponential function of *time*.[6] Generalizing this to a three-mass system, each tether length must increase exponentially with time and $l_1/l_2 = l_{sk1}/l_{sk2}$ (fully deployed tether lengths) in order to maintain the mass m_2 at the C.M. The exponentially increasing phase (acceleration phase) is followed by an exponential deceleration phase and subsequently by a transition phase to stationkeeping conditions. All the transitions between sequential phases are simultaneous for the two tethers. In the following formulas l_{I1} is the initial tether length of tether 1, l_{E1} is the tether length at the beginning of the deceleration phase, l_{T1} is the length at the beginning of the transition phase (as later explained), l_{f1} is the final length, and l_{c1} is the controlled tether length. In formulas the first two phases are summarized as follows:

Phase I (acceleration) $l_{I1} \le l_{c1} < l_{E1}$

$$l_{c1} = l_{I1}e^{\alpha t}$$

$$l_{c2} = l_{I2}e^{\alpha t} \qquad (40)$$

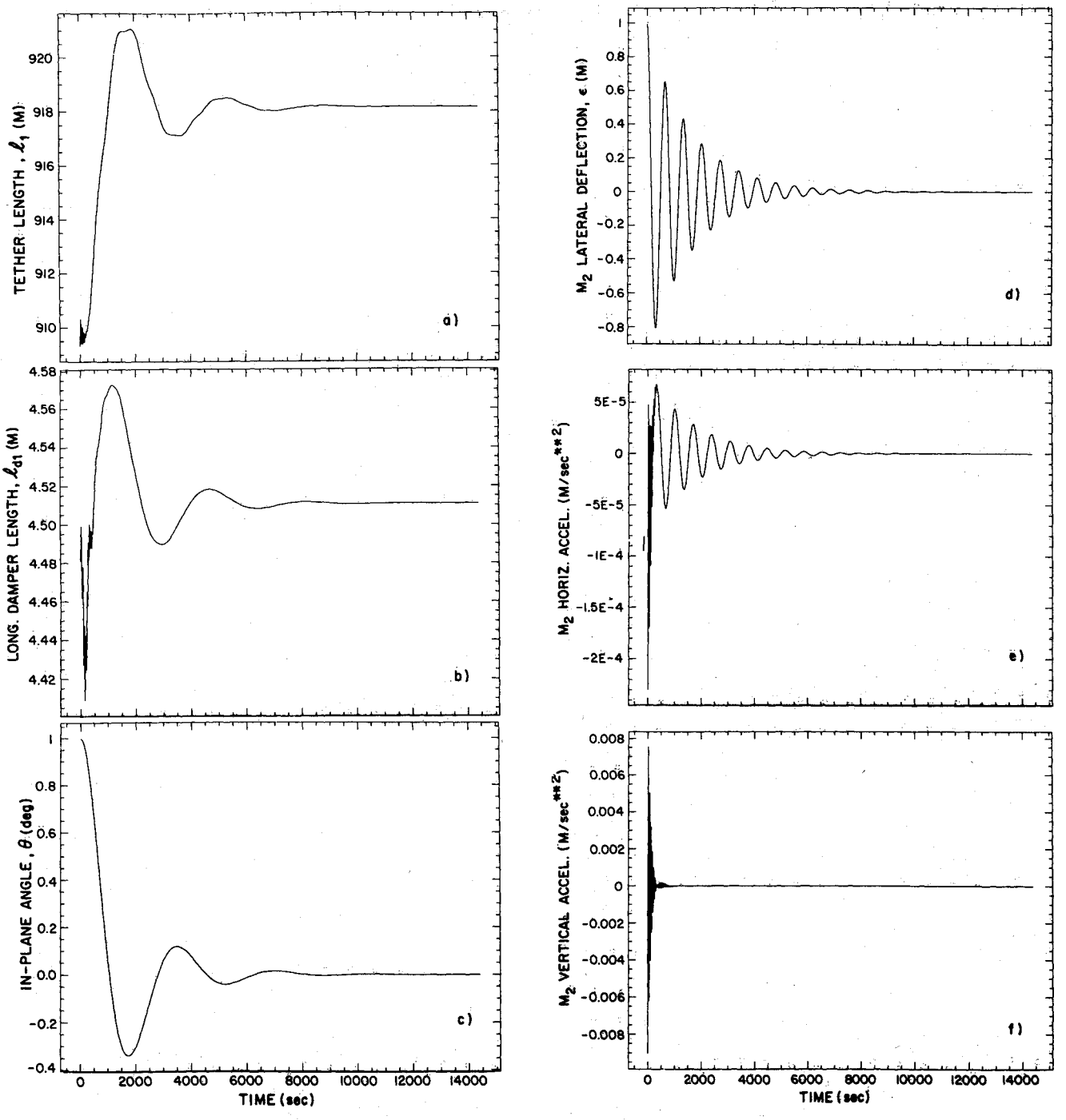

Fig. 4 Dynamics of three-mass tethered system during stationkeeping. 1 orbit = 5677 s.

Phase II (deceleration) $l_{E1} \le l_{c1} < l_{T1}$

$$l_{c1} = (l_{T1} - l_{f1})e^{-\beta t} + l_{f1}$$

$$l_{c2} = (l_{T2} - l_{f2})e^{-\beta t} + l_{f2} \tag{41}$$

where $\beta = \alpha/(l_{f1}/l_{T1} - 1)$ and $\alpha = \frac{3}{4}\,\Omega \sin(2\theta_c)$. In Eqs. (39), θ_c is the constant value of θ during the acceleration phase.

The final tether lengths l_{f1} and l_{f2} are the tether lengths at which the tether speed would be reduced to zero if the deceleration phase were continued indefinitely. In order to speed up the deceleration phase, $l_{f1} > l_{sk1}$ and $l_{f2} > l_{sk2}$.

The transition control law is activated when the actual speed of tether 1 during the deceleration phase equals the tether speed imposed by the stationkeeping control law with a libration angular rate $\dot{\theta}_T$ at the time of transition between the two phases, as set forth in the formula

$$-\beta(l_{c1} - l_{f1}) = l_{sk1} k_\theta \dot{\theta}_T \tag{42}$$

and similarly for tether 2. However, tether speed continuity does not imply tether length continuity. The mismatch is corrected by the transition control law and by a choice of control parameters that minimizes such mismatch. The transition control law is a semicycle of a cosinusoidal function of duration ΔT activated at the transition time. In formulas

Phase III (transition) $l_{T1} \le l_{c1}$

$$l_{c1} = l_{sk1}(1 - f_T - k_\theta \theta)$$

$$f_T = f_{0T} \cos\left(\frac{\pi}{2} \frac{t}{\Delta T}\right) \tag{43}$$

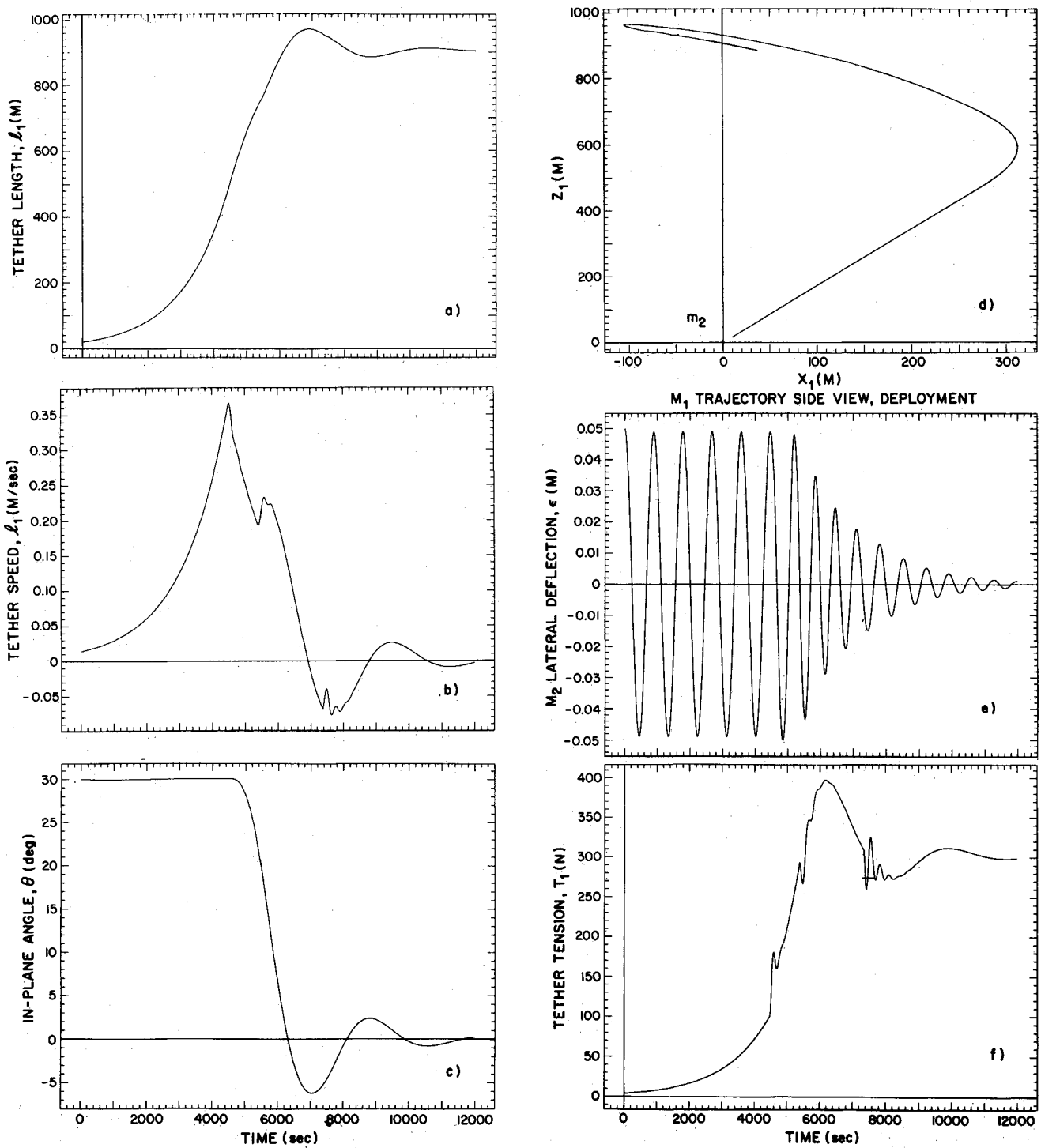

Fig. 5 Dynamics of three-mass tethered system during deployment. 1 orbit = 5677 s.

where $f_{0T} = \Delta l / l_{sk1}$ is the tether length mismatch at transition divided by the stationkeeping tether length. Similar formulas apply to tether 2.

This deployment strategy is similar to the one formulated by Misra and Modi.[8] Unlike the deployment strategy of that paper, the measurement of the libration angle θ is not required during the acceleration phase of our deployment maneuver. Consequently radar tracking is not necessary at short distances where the radar is blind. Secondly, the librational damper is activated before the end of deployment and remains active during the following stationkeeping phase when damping of librations is also necessary. In the above-mentioned reference, on the contrary, the damping of librations is proportional to the deployment speed and it tends to zero at the end of the deployment maneuver.

Numerical Simulation

Stationkeeping Phase

The effectiveness of the dampers during stationkeeping is shown in the following set of plots. These plots have been obtained by simulating the dynamic response of the constellation for 14,000 s during the stationkeeping phase under the following initial conditions: the initial tether lengths are $l_{I1} = 909$ *m* and $l_{I2} = 9090$ *m*, the initial libration angle is $\theta_I = 1$ deg, and the initial lateral deflection of mass m_2 is $\epsilon_I = 0.10$ *m*. Figures 4a and 4b show the tether length and the longitudinal damper

length, respectively, for tether 1. The same quantities for tether 2 have a similar time dependence but are scaled up a factor of 10. Figures 4c and 4d show the libration angle θ and the lateral deflection ϵ, respectively. Finally, Figs. 4e and 4f show the horizontal and vertical acceleration components measured on board the g-laboratory. Initial transients are effectively abated and, at the end of the simulation, the acceleration level at the g-laboratory (*in the absence of external forcing terms*) is well below 10^{-8} g.

Deployment Phase

The parameters for the deployment maneuver adopted in this study have been obtained by trial and error after several deployment simulation runs. The following set of parameters provides a stable, fast maneuver and minimizes the mismatch at the transition between the deployment and stationkeeping phases. The parameters are as follows:

$$l_{E1} = 500 \text{ m}$$

$$l_{f1} = l_{sk1} + \sigma = 909 + 100 = 1009 \text{ m}$$

$$\theta_c = 30 \text{ deg}$$

$$\Delta T = 2000 \text{ s} \qquad (44)$$

In the deployment maneuver simulation shown here the initial tether lengths are $l_{I1} = 20$ m, $l_{I2} = 200$ m. Although these values are greater than in actuality, they allow a deployment without tether slackenings. The system shows a tendency to go temporarily slack at the very beginning of the deployment maneuver because of small errors in the initial conditions. An in-line thruster, as also proposed by Banerjee and Kane[9] and adaptive longitudinal dampers can help considerably in relieving the slack tether problem but were not included in this study. An initial libration angle $\theta_I = 30$ deg and an alignment error of the three masses $\epsilon_I = 0.05$ m complete the set of initial conditions. The dynamic response, however, is fairly insensitive to these parameters. Figures 5a and 5b show the tether length and tether speed respectively of tether 1 vs time. The corresponding quantities for tether 2 are like those of tether 1 scaled up by a factor of 10 (they are not shown here for brevity's sake). The deployment is completed in approximately 3 h. This value, however, is affected by the initial tether length and is therefore ultimately affected by the position of the reeling system on the Space Station with respect to the Station C.M. More important are the initial tether speeds which must be as close as possible to the initial design speeds, according to the law $l_{Ii} = \alpha l_{fi}$, in order to avoid slackening of the tethers. In Fig. 5b the different phases of the deployment control law are evident: the activation of the rotational damper results in the ripple at approximately 5500 s, while the disactivation results in the second ripple at 7500 s. The time history of the libration angle θ is plotted in Fig. 5c, where the θ angle is constantly equal to θ_c, as expected, during the deployment acceleration phase. Figure 5d shows the side view of the trajectory of mass 1 (Space Station) with respect to the system center of mass. Mass 3 (the end platform) follows a mirrorlike trajectory scaled up by a factor of 10. Mass 2 (the g-laboratory) remains very close to the system C.M. throughout the deployment maneuver. Figure 5e is the lateral displacement ϵ of mass 2 vs time. When the librational/lateral damper is switched on at 5500 s this oscillation begins to be damped out. The damping of ϵ is less effective than that of the angle θ because the librational/lateral damper is tuned to the librational frequency. By using a multifrequency damping technique, as formulated in Eqs. (36), the damping of the lateral oscillation can be further improved. Figure 5f shows the time history of the tension in tether 1 which is very close to that of tether 2 throughout the entire deployment maneuver.

Conclusions

The proposed tethered system is an advisable alternative to the presently contemplated micro-g laboratory installed near the Space Station C.M. The low frequencies of the long tethers and associated dampers provide a good isolation from Space Station and/or end platform oscillations at a frequency higher than 0.1 Hz (it is possible to improve even further on this score). The tether system has the additional capability of controlling the position of the g-laboratory along the tether in order to nullify the gravity gradient or to vary it according to a prescribed profile. The proposed deployment strategy allows the system to reach its final configuration in approximately 3 h. The initial part of deployment, however, requries a more detailed analysis. The active and passive dampers added to the system provide an effective abatement of the longitudinal, librational, and lateral oscillations, as demonstrated by the simulations of the deployment and stationkeeping phase. A thorough analysis of the perturbations acting upon the system is yet required. It will be a topic of investigation in our future studies.

Acknowledgments

Acknowledgment is made to Dr. Georg von Tiesenhausen, NASA/MSFC and Mr. William O. Nobles, Martin Marietta Aerospace, who participated in originating the idea of a three-mass tethered g-laboratory. Dr. Georg von Tiesenhausen also supported the dynamics analysis of the system, NASA/MSFC Contract NAS8-36606.

References

[1]Sharpe, A. (Ed). "Low Acceleration Characterization of Space Station Environment," Teledyne Brown Engineering, Final Report for NASA/MSFC Contract NAS8-36122, Mod. 6, Oct. 1985.

[2]Baugher, C.R. (Ed). "Micro-g Requirements Analysis, Space Station RUR-2," EMS Product, Report for NASA/MSFC, WP01, EMS R5.1.4, Aug. 1985.

[3]Carruthers, J. R., "Acceleration Level Requirements for Microgravity Science on the Space Station," INTEL, Report for NASA/MSFC, May 1985.

[4]Lorenzini, E. C., "Analytical Investigation of the Dynamics of Tethered Constellations in Earth Orbit," SAO, Final Report for NASA/MSFC under Contract NAS8-35497, Dec. 1984.

[5]Bekey, I., "Tethers Open New Space Options," *Astronautics and Aeronautics*, April 1983.

[6]Baker, W. P. et al., "Tethered Subsatellite Study," NASA TMX-73314, March 1976.

[7]Spencer, T. M., "Atmospheric Perturbation and Control of a Shuttle/Tethered Satellite," Proceeding of the 8th IFAC Symposium on "Automatic Control in Space," Sept. 1980.

[8]Misra, A. K. and Modi, V. J., "Deployment and Retrieval of Shuttle Supported Tethered Satellites," *Journal of Guidance, Control and Dynamics*, Vol. 5, No. 3, May-June 1982, pp. 278-285.

[9]Banerjee, A. K. and Kane, T. R., "Tethered Satellite Retrieval with Thruster Augmented Control," *Journal of Guidance, Control and Dynamics*, Vol. 7, No. 1, Jan.-Feb. 1984, pp. 45-50.